JOURNAL OF MATERIALS SCIENCE 27 (1992) 3231–3238

Synthesis of Si(C, N) nanoparticles by rapid laser polycondensation/crosslinking reactions of an organosilazane precursor

K. E. GONSALVES*, P. R. STRUTT‡, T. D. XIAO‡, P. G. KLEMENS§
* *Department of Chemistry and Polymer Science Program,* ‡ *Department of Metallurgy, and* § *Department of Physics; University of Connecticut, Storrs, CT 06269, USA*

A study has been made of basic mechanisms involved in the rapid synthesis of pre-ceramic and ceramic nanoparticle powders. In this process an aerosol, formed from an ultrasonically atomized liquid organosilazane monomer, $[CH_3SiHNH]_n$, is injected into the beam of an industrial CW CO_2 laser. One critical feature examined was the rapid condensation of molecular species from the laser plume, in a process involving three-dimensional crosslinking polycondensation reactions. In accompanying studies, a model has been formulated to determine the laser plume temperature, the cooling rate of condensing species and the particle diameter. These are obtained by analytical solution of heat conduction, momentum and mass conservation equations that consider heat loss by gas conduction, radiation, evaporation and convection.

1. Introduction

There is considerable interest in the development of high temperature, high strength composite materials, that exhibit resistance to corrosion, oxidation and thermal shock [1]. The objective of this current research is to develop organometallic/polymeric precursors for ceramic, intermetallic and composite materials. Previous studies have demonstrated the feasibility of using such precursors for producing Ti(C, N) in polymer matrices [2], and liquid polysilazanes for the synthesis of ultrafine powders and films [3–5]. Blends of silazane oligomers and titanium dialkylamides have also been utilized by us as precursors for coating carbon–carbon fabrics/composites [6]. Cyclopentadienylcycloheptatrienyl titanium has also been used as a precursor to deposit Ti(C, O) on polyimide substrates at temperatures below 300 °C [7]. The synthesis of iron–cobalt intermetallics has also been reported [8].

It has been recognized [9] that ceramic and metallic materials with novel properties are obtained when the constituent phase morphology is reduced to nanometre dimensions (5–100 nm). Currently, the synthesis of nanomaterials is being addressed by using physical methods. Since these involve particularly slow rate processes, they do not provide a viable approach for the eventual production of significant quantities of material. To overcome this limitation, a methodology has now been developed [10] using a synergistic approach, involving organometallic/polymer chemistry and materials processing concepts.

The new technique involves using molecular precursors that facilitate the synthesis of nanomaterials containing phases of desired composition and crystal structure. Metalorganic/polymeric precursors are particularly attractive since they can be used to: (1) yield a high fraction of end product and (2) obtain phases with a selected stoichiometry. Consequently, the possibility now exists for producing nanocomposite materials in significant amounts. These may contain a diverse range of phases such as intermetallic, silicide, boride, nitride, carbide and oxide phases.

This paper now reports a technique developed for the ultra-rapid conversion of a liquid silazane monomeric precursor to intermediate polymeric pre-ceramic Si–C–N containing nanoparticles. This occurs by laser-induced polycondensation and crosslinking reactions using ultrasonic injection of a liquid precursor into the beam of a high powered industrial CO_2 laser. The pre-ceramic powder produced this way, can either undergo *in situ* laser consolidation into a ceramic coating, or be collected for processing into bulk material.

2. Experimental procedure

2.1. Precursor synthesis

The liquid silazane was prepared by the ammonolysis of methyldichlorosilane according to the procedure [11]. Diethyl ether and methyldichlorosilane were cannulated into a flask cooled to 0 °C in an ice bath. An excess of anhydrous ammonia was bubbled into the reaction mixture with vigorous stirring until strongly basic. The reaction mixture was stirred for another 2 h and then filtered under argon. The solvent was removed by trap-to-trap distillation under vacuum leaving an oily residue. The ammonolysis products consist of mainly cyclics $[CH_3SiHNH]_x$ with $x = 3$ or 4 as well as some linear structures, the

0022–2461

major component being the $x = 4$ cyclic [11]. The molecular weight determined by cryoscopy in benzene was 298 g mol^{-1}. The structure of the cyclic silazanes is depicted in Fig. 1 and its infrared (i.r.) spectrum in Fig. 2.

Fourier transform infrared (FTIR) spectroscopy of the precursor revealed a strong absorption peak in the 10.6 μm wavelength region. From absorption measurements on a series of samples, with varying dilution in benzene, it was observed that Beers law $I = I_0 \exp(-ax)$ was obeyed. The term a, is the extinction coefficient and x is the liquid depth. The value of a at a wavelength of 941 cm^{-1} (or 10.6 μm) was 45.2 cm^{-1}. This indicated that 95% of the radiation was absorbed within a depth of 11 μm.

2.2. Laser processing

The version of the laser processing method used to produce *in situ* ceramic coatings is shown schematically in Fig. 3. A window at the top of the chamber provides access for a convergently focused beam of a high power CW CO_2 laser. The CW control laser used has a maximum power of 2.3 kW; however, the power level maintained in the current study was 700 W. Specific care was taken to minimize redirected beam power density within the chamber, due to reaction product deposition on the entry window. This was achieved by allowing the beam to pass through a small chamber maintained at a small excess pressure, before entering the main chamber. A side window providing a view of the rotation stage (with mounted substrate), and the ultrasonic nozzle (Sono-Tek) facilitates observation of process phenomena. In the experiments, substrates used for depositing ceramic layers were nickel discs of 1.2 cm diameter and 2 mm thickness.

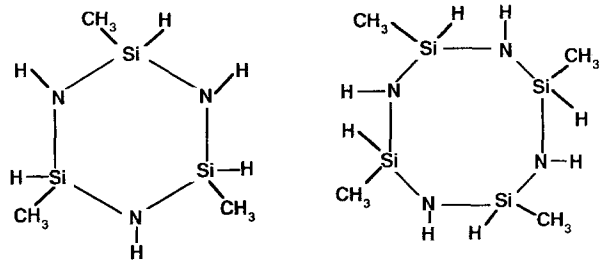

Figure 1 Molecular structure of silazane precursor.

The processing procedure first involved filling the ultrasonic atomizer supply chamber with liquid precursor. During process operation, this liquid was forced into the nozzle by applying an argon gas pressure differential. The magnitude of this controlled pressure differential determined the precursor delivery rate from the nozzle. In the present study this was 8.3×10^{-3} cm^3 s^{-1}. Following this step, the chamber was flushed and back-filled with nitrogen to a pressure of 1×10^5 Pa. Ten minutes prior to processing, and throughout the process cycle, it was fed with ammonia and helium, at flow rates of 150 and 100 sccm (standard cm^3 s^{-1}), respectively. This condition was maintained using MKS gasflow controllers.

The focused laser beam diameter at the substrate surface was approximately 1.3 cm, with a beam power of 700 W, the corresponding power density was approximately 5.3×10^2 W cm^{-2}. As shown in Fig. 3, the precursor aerosol injected into the beam–substrate interaction region forms a luminous plume as measured by an optical pyrometer, the plume temperature is approximately 2000 K.

3. Results and discussion

The structure of the liquid silazane precursor used to synthesize the pre-ceramics, which can eventually produce Si_3N_4/SiC ceramics, is shown in Fig. 1. This was

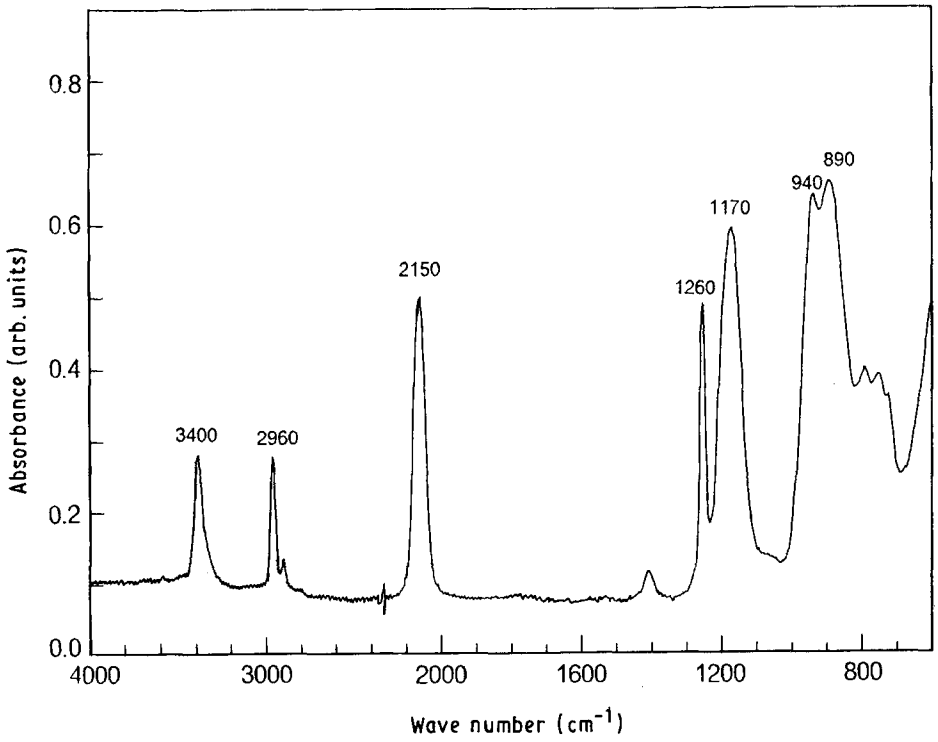

Figure 2 Infrared spectrum of precursor.

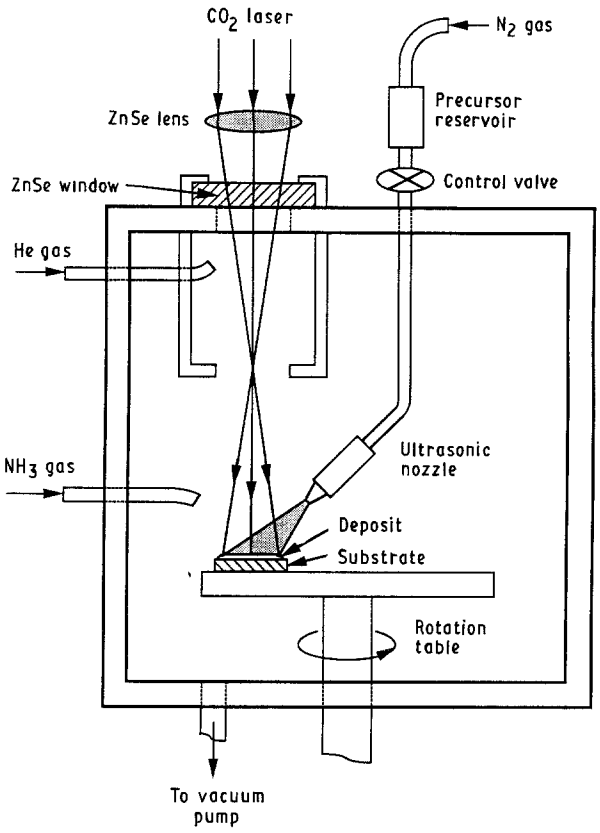

Figure 3 Schematic diagram of laser processing chamber.

prepared by the ammonolysis of methyl dichlorosilane according to the method of Seyferth and Wiseman [11]. The precursor is a mixture of six and eight member rings with some linear oligomers also present. The number average molecular weight of the liquid silazane precursor was 298 g mol^{-1}, determined by cryoscopy in benzene. The infrared spectrum of the silazane revealed a strong absorption peak in the 10.6 μm wavelength region. This ensures strong energy transfer when a precursor aerosol is injected into the beam of CO_2 laser as depicted in Fig. 2. An important feature of this silazane precursor is the high degree of reactivity in the Si–H and N–H functionalities, which is a key feature in its rapid crosslinking during processing [11].

As previously mentioned, the technique may be used to synthesize: (1) pre-ceramic nanoscale powders, and (2) ceramic deposited layers. These two basic modes are conceptualized in Fig. 4a and b. These in effect represent the phenomena occurring in the laser–substrate interaction region in Fig. 3. Strong energy coupling between the laser beam and the injected aerosol droplets results in their rapid evaporation and the formation of a plume (or plasma). The precursor molecular groups formed by the process, rapidly cool as they emerge from the plume. Rapid condensation and crosslinking from the plume is intriguing, since strong crosslinking leads to the formation of intermediate precursor particles with a mean diameter of 60 nm. This rapid polymerization process leading to nanoparticles does not occur *via* conventional chemical processing. In Fig. 4b, the intermediate precursor particles form on a cold collector surrounding the plume. Careful removal of the powder from the collector, shows that 70 wt % of the liquid precursor is converted into nanoparticle powders. A rate of production of approximately 100 g h^{-1} has been achieved.

As mentioned above, nanoparticles may be collected on a laser-heated substrate (Fig. 4a) to undergo coalescence to form a deposited pre-ceramic layer. Coalescence (or sintering) is driven by the high surface area of the nanoparticles and very short diffusion distances. Consequently, as depicted in Fig. 4a, consolidation as well as synthesis can occur in an integrated process, thus obviating the need to handle the nanoparticle powders. However, the method may be used expressly for powder synthesis.

Structural examination of powders using FTIR spectroscopy reveal a partial elimination of methyl groups with evidence of crosslinking. Transmission electron microscopy (TEM) indicates that the particles are highly transparent and dispaly no evidence of

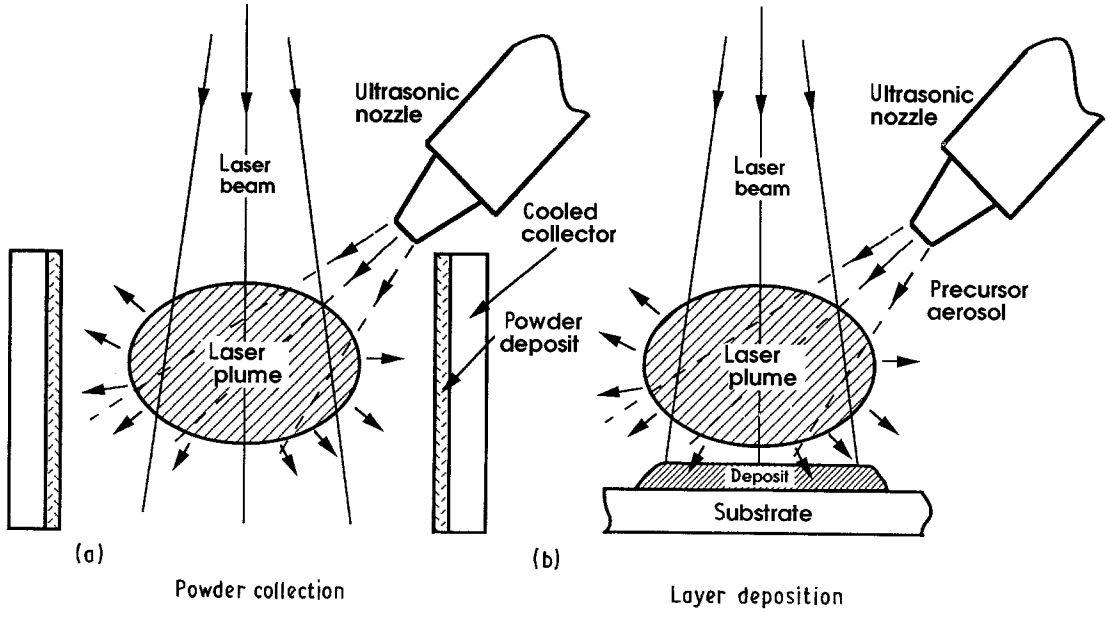

Figure 4 Use of laser processing for: (a) powder synthesis, and (b) surface layer deposition.

porosity. As shown by thermogravimetric analysis (TGA) Fig. 5, conversion of nanoparticle powder to the end product, namely Si_3N_4/SiC, involves an approximately 10% weight loss (curve 1), whereas the TGA of the unprocessed monomer leaves behind a residue of only 10% (curve 2) as reported earlier [11]. The differential scanning calorimetry (DSC), Fig. 6, of the powders also indicates that extensive crosslinking has occurred by the absence of a melting transition, T_m. No obvious glass transition, T_g, could be discerned in the DSC profile. The crosslinked pre-ceramic powders were extracted with chloroform and the ^1H nuclear magnetic resonance (NMR) spectrum of the soluble fraction indicated that the NH groups were in considerable excess of methyl and Si–H groups. The excess of NH groups can be explained *via* a nucleophilic cleavage of CH_3 groups from silicon in the precursor, in the presence of ammonia [10] resulting in the possible introduction of active $-Si-NH_2$ functionalities. These reactive groups could be responsible for the extensive crosslinking mechanisms by further nucleophilic displacements on neighbouring atoms

$$-Si-CH_3 + NH_3 \rightarrow -Si-NH_2 + CH_4$$

These extensive crosslinking mechanisms could result initially in highly branched structures [10–12], eventually leading to 3D structures as observed in conventional organic gel formation polymerizations. Similar results as shown in the above chemical representation, were obtained by us in the chemical vapour deposition (CVD) of these precursors in ammonia [13].

The structural characteristics of the powders were examined by scanning electron microscopy (SEM) and transmission electron microscopy (TEM). Fig. 7 shows untransformed pre-ceramic particles which were collected on a cold substrate. In this TEM, the pre-ceramic particles are supported on a carbon film. This micrograph shows the transparency of the individual particles and the dark contrast that arises from particle overlapping. Electron diffraction reveals the particles to be entirely amorphous. These particles were subsequently heat treated in an ammonia atmosphere (flow rate 100 sccm) from ambient to 1100 °C. Fig. 8 is a micrograph of a typical sample annealed at 1100 °C in ammonia for 6 h. Particle size analyses of the pre-ceramics and the annealed samples were conducted. The samples were prepared by two methods: 1. using a replication technique in which the pre-ceramic particles were extracted from the chamber

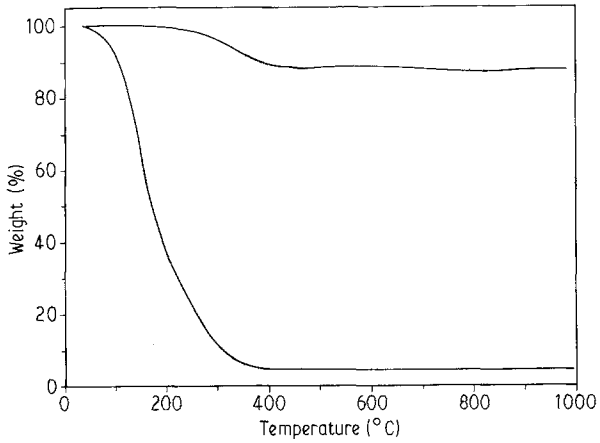

Figure 5 Thermogravimetric curve for conversion of pre-ceramic powders to ceramic.

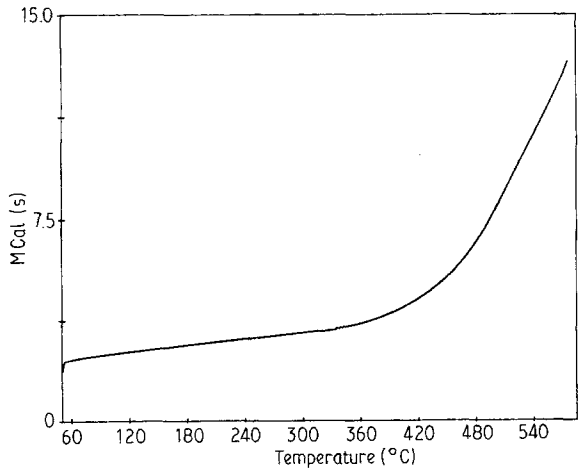

Figure 6 Differential scanning calorimetry curve (scan rate = 10.0 deg min^{-1}).

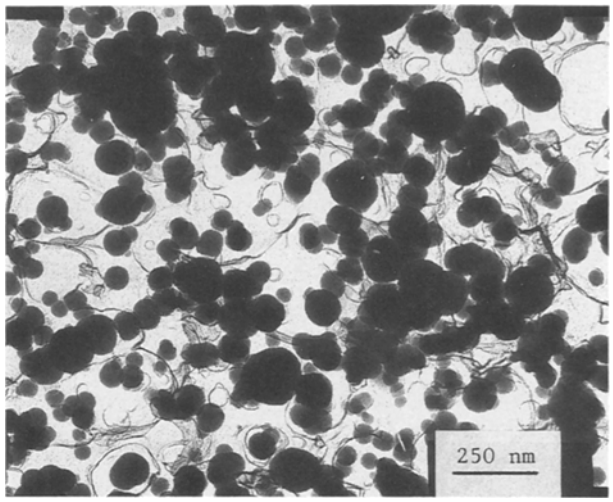

Figure 7 TEM micrograph of pre-ceramic nanoparticles.

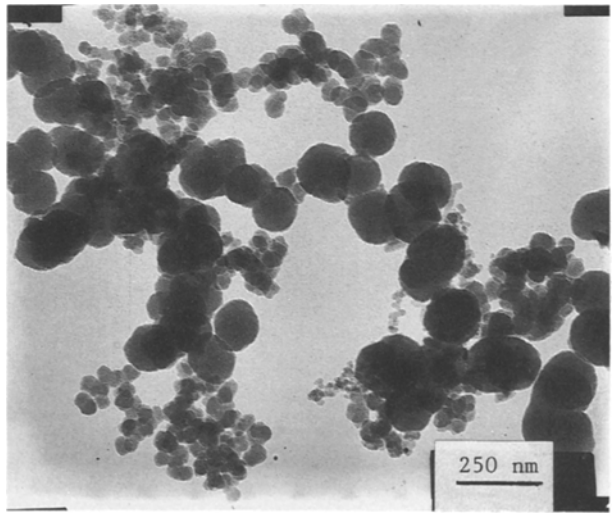

Figure 8 TEM micrograph of thermally transformed pre-ceramic particles.

walls, and 2. a solution technique in which the powders were dispersed in dried, deoxygenated methanol using an ultrasonic vibrator. These particles were then transferred on to a TEM grid, 200 mesh size coated with carbon film, by dipping it into the above dispersion. These coated grids were examined using a TEM (Philips 300 and 420), at an acceleration voltage of 100 keV. The TEM micrographs were magnified 2 to 3 times and the particle diameters measured using a magnified ruler (0.1 mm accuracy). TEM micrographs of the samples were then taken randomly. The total number of particles counted for both the pre-ceramics and ceramics were 423. The mean diameter of the pre-ceramic particles was 62 nm. The particle size distribution of the ceramic powders showed a bimodal distribution: first mode, mean diameter 44.8 nm: second mode, mean diameter 119.43 nm. The shrinkage of the pre-ceramic particles can be explained by the loss of the methyl groups resulting in enhanced cross-linking to eventually form silicon nitride nanoparticles. The larger size particles can be attributed to coalescence of the pre-ceramic particles during sintering. The particle size distribution curves for the pre-ceramic and ceramic particles are shown in Fig. 9.

In order to obtain maximum information on the evolution of the ceramic particles from the pre-ceramic polycondensates/crosslinked gels, FTIR analysis was carried out using a KBr pellet. The pre-ceramic powders were annealed in two gas environments and the temperature varied from 500 to 1100 °C. Careful examination revealed that the following bonds were present in the pre-ceramic powder: N–H at 3410 cm^{-1}, Si–H at 2200 cm^{-1}, C–H at 2960 cm^{-1}, Si–CH_3 at 1260 cm^{-1}, Si–N at 460 cm^{-1} and a broad band from 800–1100 cm^{-1}. This could be due to a combination of Si–C, Si–N, N–H and Si–O bonds. We have observed that traces of oxygen are unavoidable despite stringent precautions. It is pertinent to mention that the FTIR spectrum of the crosslinked pre-ceramic is quite similar to that of the silazane monomer, except that the Si–H and Si–CH_3 peaks in the pre-ceramic are diminished and the Si–N peaks increased relative to those of the monomer silazane. When the powders were annealed in ammonia at 550 °C, the FTIR spectrum indicated that the intensity of the C–H and Si–H peaks decreased, and at 800 °C the Si–CH_3 peak disappeared completely. After a temperature of 1000 °C, a pronounced peak at 960 cm^{-1} indicated the presence of silicon nitride. When a similar treatment was carried out in nitrogen, the corresponding absorption peak was observed at 1090 cm^{-1}, which can be attributed to a combination of Si_3N_4 and SiC bonds. The FTIR spectra of the annealing processes in ammonia and argon are depicted in Figs 10 and 11. Elemental analysis of these powders also confirmed that in ammonia, essentially Si, N with smaller amounts of carbon and oxygen were present. In argon the carbon was present to a larger extent.

As mentioned above, the above process can also be used for the synthesis of pre-ceramic films which on annealing in ammonia result in the formation of Si_3N_4. Fig. 12 is the surface view of a coating produced when pre-ceramic, i.e. crosslinked polysilazanes are deposited on a hot nickel substrate. The thermal effect of laser heating is to promote inter-particle sintering. Clear evidence of coalescence is visible in the higher magnification SEM in Fig. 13. The cross-sectional view of a deposited layer in Fig. 14 reveals the excellent bonding of the pre-ceramic polymeric layer to the substrate. Subsequent heat treatment converts these pre-ceramic layers to Si(N, C) materials.

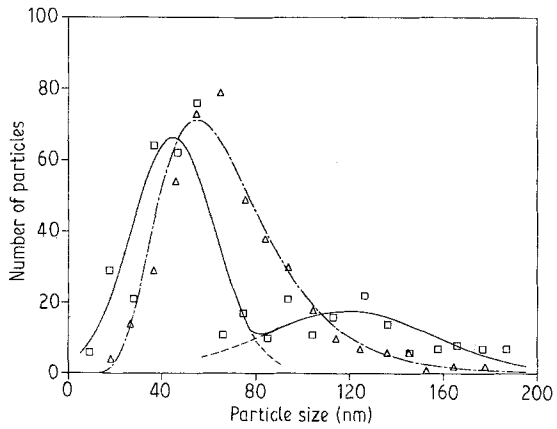

Figure 9 Particle size distribution curves for: (— — —) calculated and (△) experimental values for pre-ceramic and (—) calculated and (□) experimental values for ceramic particles.

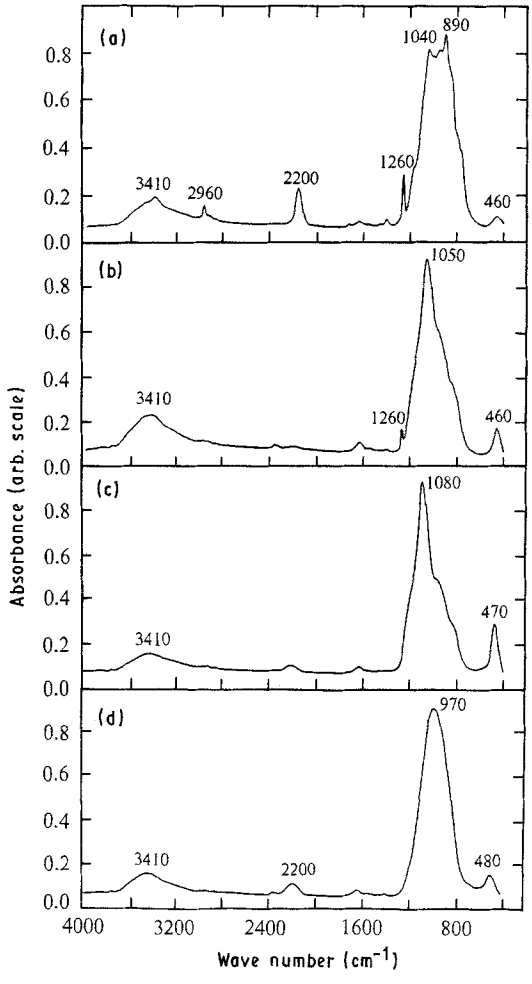

Figure 10 FTIR spectra of annealing pre-ceramic powders in ammonia: (a) no heat treatment; (b) 500; (c) 800 and (d) 1100 °C.

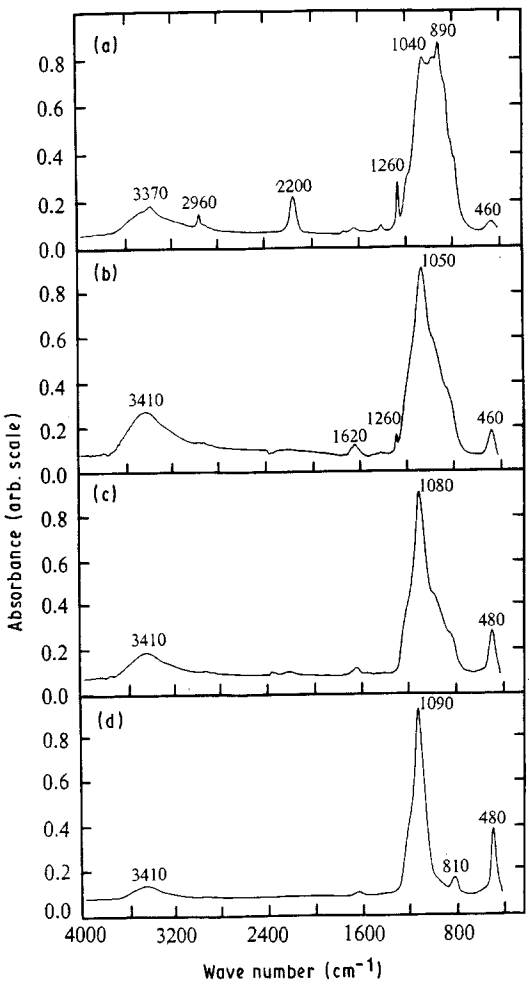

Figure 11 FTIR spectra of annealing pre-ceramic powders in argon; (a) no heat treatment; (b) 500; (c) 800 and (d) 1100 °C.

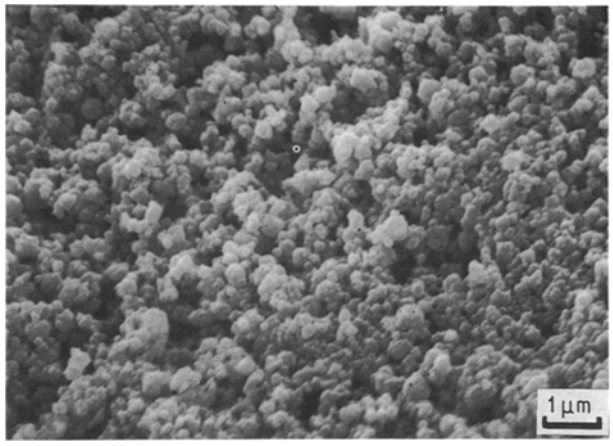

Figure 13 Higher magnification view of the deposit shown in Fig. 12, revealing interparticle coalescence.

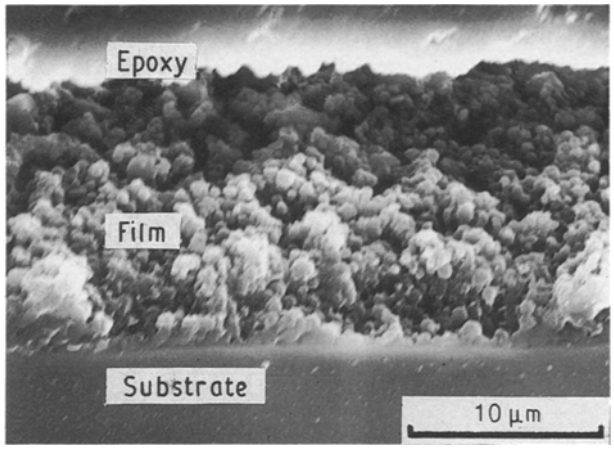

Figure 14 Cross-section view of pre-ceramic deposit on silica substrate.

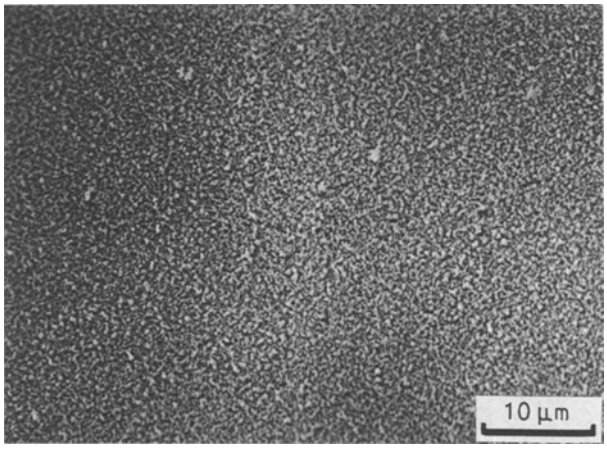

Figure 12 Surface deposit of pre-ceramic formed by rapid condensation of fine particles from the laser plume on to the laser heated substrate.

This paper so far has discussed the chemical/laser conversion of a silazane monomer to highly cross-linked pre-ceramic nanoparticles. Factors determining the nanophase particle size are considered in a theoretical model. When intense electromagnetic radiation interacts with absorbing aerosol droplets, various phenomena can occur, including thermal blooming, droplet evaporation and optical breakdown. Each of these effects is due to the absorption and consequent liberation of energy in various forms by the individual particles within the aerosol [14–17]. Chitnavis and Gerstl [18], has pointed out that the propagation of a laser beam in an aerosol can be considered to be linear for power densities less than 10^2 W cm^{-2}. The power density employed in the current study of 6.2×10^2 W cm^{-2} results in rapid evaporation of a liquid monomer precursor to form an intense plume. Condensation of precursor molecules emerging from the plume result in pre-ceramic nanophase particles.

4. Proposed model

A theoretical analysis of the laser conversion of liquid monomer to pre-ceramic particles has to consider:

1. The high driving force for this rapid process, which is created by the high temperature differential between the laser plume and its surroundings.
2. The vapour phase mechanisms involved in particle formation by molecular condensation.

First, however, it is necessary to estimate the laser plume temperature. This is obtained by equating the absorbed beam power, P, to the sum of dissipated losses due to radiation, thermal conduction, and precursor evaporation, see Equation 1

$$P = \sigma 2\pi R h T^4 + K_g 2\pi h T + \Delta H_{vap} \frac{m}{t} \quad (1)$$

where R is radius of laser plume, h its height, and m/t the

material evaporation rate. Values of the thermal conductivity, K_g, monomer vapourization energy, ΔH_{vap}, are 7.8×10^{-4} J K^{-1} cm^{-1} s^{-1} and 692.8 J g^{-1}, respectively; σ is the Stefan–Boltzmann constant (5.57×10^{-12} W cm^{-2}). Values of the second and third terms in Equation 1 of only 20 and 6 W show radiation to be the dominate energy loss. For $P = 700$ W, the plume temperature is determined to be 1960 K.

Surrounding the laser plume, there is an outward radial flow of both the host gas (ammonia and helium) and precursor vapour. In this process, the gas and vapour species are each assumed to move with velocity, v_f. To determine the value of v_f and the precursor vapour pressure P_v, it is necessary to consider the mass and momentum balance, Equations 2 and 3

$$\frac{m}{t} = A\rho_v \frac{P_v}{P} v_f \quad (2)$$

$$\frac{m}{t} v_{jet} = A\left(\rho_g \frac{P - P_v}{P} + \rho_v \frac{P_v}{P}\right) v_f^2 \quad (3)$$

Values of the precursor delivery rate (m/t), host gas density, ρ_g, and precursor vapour density, ρ_v, are 8.43×10^{-3} g s^{-1}, 0.723×10^{-4} g cm^{-3} and 18.27×10^{-4} g cm^{-3}, respectively. Also, the plume area, A, and initial aerosol velocity are 8.17 cm^2 and 33 cm s^{-1}, respectively. Combining Equations 2 and 3 we obtain the quadratic Equation 4, from which P_v/P and P_v are also obtained; P the total pressure is maintained at 1 atm.

$$A\rho_v^2 \frac{v_{jet}}{(m/t)} (P_v/P)^2 + (\rho_g - \rho_v)(P_v/P) - \rho_g = 0 \quad (4)$$

Using the given parametric values, v_f and P_v are determined to be 15.9 cm s^{-1} and 0.035 atm, respectively.

The cooling rate dT/dt as the hot vapour flows to cooler regions with velocity v_f, is given by Equation 5

$$\frac{dT}{dt} = \frac{dT}{dr} v_f \quad (5)$$

With determined values of the plume temperature, T_o, and v_f of 1960 K and 15.9 cm s^{-1}, and $R = 0.65$ cm, the value of dT/dt is 4.8×10^4 K s^{-1}, and the cooling time is 6.25×10^{-3} s. During the cooling, each outward diffusing precursor molecule sweeps out a volume $\sigma_c vt$, where σ_c is the molecular cross-section, and t the cooling time. The molecules that condense are contained in a volume of $(Dt)^{3/2}$, where D is the diffusivity, v is the root mean square molecular speed. Thus, the probability that any molecule hits the nucleus is

$$P = \frac{\sigma_c vt}{(Dt)^{3/2}} \quad (6)$$

If there are N molecules, each of volume a^3, in the diffusion accessible volume $(Dt)^{3/2}$, the volume of the condensate becomes

$$V = PNa^3 = \sigma_c vt \frac{\rho_v}{\rho_s} \quad (7)$$

Here ρ_s is the density of the solid, and ρ_v/ρ_s is usually in the order of 3×10^{-4}. The cross-section σ_c is estimated to be 4×10^{-15} cm^2, and v is estimated to be 1.1×10^5 cm s^{-1}. Therefore the volume of a condensed particle is determined to be 5.72×10^{-16} cm^3, which corresponds to a diameter of 93 nm.

Microstructural analysis shows the smallest condensate diameter, within a particle size distribution having a mean diameter of 62 nm, is 18.5 nm. As revealed by transmission electron microscopy, the larger diameter particles appear to form by smaller particle coalescence. A critical factor in the theoretical overestimate of the condensed particle diameter (by a factor of 5) is the assumption of unity sticking coefficient. Clearly, in practice this value may be reduced significantly. Analysis of this factor is being considered in a development of the present model.

5. Conclusion

We have thus developed a process for the laser conversion of liquid silazane precursor into pre-ceramic, i.e. highly crosslinked polysilazane powders. These powders may be converted into Si_3N_4/SiC ceramic nanoparticle powders which can then be consolidated by hot isostatic pressing (HIP). Alternatively, they can be die-extruded into pre-ceramic preforms of a component prior to thermal conversion into a desired product. Furthermore, the laser method of producing the pre-ceramic material from organometallic liquid monomers is in principle ideally suited for direct component fabrication, this methodology involving laser beam scanning and computer control. This work emphasizes the merits of a synergistic approach involving organometallic/polymer chemistry and material processing. We are presently studying the crosslinking mechanisms involved in the formation of the pre-ceramics by solid state ^{29}Si, ^{13}C CP–MAS NMR spectroscopic methods. Direct thermal methods for obtaining the nanoparticle pre-ceramics are also being developed.

Acknowledgement

Acknowledgement is made to the University of Connecticut Research Foundation for partial support of this project.

References

1. K. E. GONSALVES, in "Inorganic and Metal Containing Polymeric Materials", edited by J. E. Sheats, C. E. Carraher Jr, C. U. Pittman Jr, M. Zeldin and B. Currell (Plenum Press, 1991) p. 173.
2. K. E. GONSALVES and R. AGARWAL, *J. Appl. Polym. Sci.* **36** (1988) 1659.
3. T. D. XIAO, P. R. STRUTT and K. E. GONSALVES, *Mat. Res. Soc. Symp. Ser.* **155** (1989) 247.
4. P. R. STRUTT, K. E. GONSALVES and A. P. MAGEE, *Chem. Mater.* **2** (1990) 232.
5. T. D. XIAO, P. R. STRUTT and K. E. GONSALVES, *Mat. Res. Soc. Symp. Ser.* **168** (1990) 199.
6. K. E. GONSALVES and R. YAZICI, *J. Mater. Sci. Lett.* **10** (1991) 834.
7. K. E. GONSALVES and M. D. RAUSCH, *Inorg. Orgmet. Polym.* **1** (1991) 131.

8. K. E. GONSALVES and K. T. KEMBAIYAN, *J. Mater. Sci. Lett.* **9** (1989) 659.
9. B. H. KEAR, L. E. CROSS, J. K. KEEM, R. W. SIEGEL, F. SPAEPEN, E. L. THOMAS and K. N. TU, in "Research Applications for Materials with Ultrafine Structures" (National Academy Press, Washington, 1989).
10. K. E. GONSALVES, P. R. STRUTT and T. D. XIAO, *Adv. Mater.* **3** (4) (1990) 202.
11. D. SEYFERTH and G. H. WISEMAN, *J. Amer. Ceram. Soc.* **67** (1984) C-132.
12. D. SEYFERTH, G. H. WISEMAN, J. M. SCHWARK, Y. Yu and C. A. POUTASSE, in "Inorganic and Organometallic Polymers" edited by M. Zeldin, K. J. Wynne and H. Allcock, ACS Symposium Series no. 360 (American Ceramic Society, Washington DC, 1988) p. 143.
13. Y. W. BAE, H. DU, B. GALLOIS, K. E. GONSALVES and B. J. WILKENS, *Chem. Mater.*, submitted.
14. S. C. DAVIS and J. R. BROCK, *Appl. Opt.* **26** (1987) 786.
15. R. L. ARMSTRONG, *ibid.* **26** (1987) 533.
16. D. R. ALEXANDER and J. G. ARMSTRONG, *ibid.* **26** (1987) 533.
17. F. A. WILLIAMS, *J. Heat Mass Trans.* **8** (1965) 575.
18. S. M. CHITNAVIS and S. A. W. GERSTL, *J. Appl. Phys.* **62** (1987) 3091.

Received 20 February
and accepted 24 April 1991